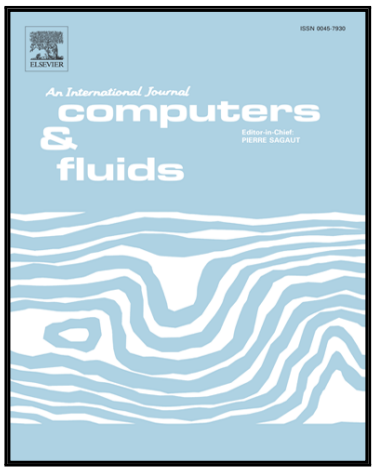

A Stochastic Multiple Mapping Conditioning Computational Model in OpenFOAM for Turbulent Combustion

S. Galindo-Lopez, F. Salehi, M.J. Cleary, A.R. Masri, G. Neuber, O.T. Stein, A. Kronenburg, A. Varna, E.R. Hawkes, B. Sundaram, A.Y. Klimenko, Y. Ge

PII: S0045-7930(18)30187-7
DOI: 10.1016/j.compfluid.2018.03.083
Reference: CAF 3844

To appear in: *Computers and Fluids*

Received date: 28 September 2017
Revised date: 5 March 2018
Accepted date: 30 March 2018

Please cite this article as: S. Galindo-Lopez, F. Salehi, M.J. Cleary, A.R. Masri, G. Neuber, O.T. Stein, A. Kronenburg, A. Varna, E.R. Hawkes, B. Sundaram, A.Y. Klimenko, Y. Ge, A Stochastic Multiple Mapping Conditioning Computational Model in OpenFOAM for Turbulent Combustion, *Computers and Fluids* (2018), doi: 10.1016/j.compfluid.2018.03.083

Highlights

- Stochastic MMC-LES and MMC-RANS are implemented into OpenFOAM.
- Code architecture is based on layered template classes and abstract sub-models.
- Mass consistency of the hybrid Eulerian and Lagrangian schemes is demonstrated.
- Numerical convergence with increasing stochastic particles is demonstrated.
- Numerical convergence with increasing aerosol species sections is demonstrated.

A Stochastic Multiple Mapping Conditioning Computational Model in OpenFOAM for Turbulent Combustion

S. Galindo-Lopez[a], F. Salehi[b], M. J. Cleary[a,*], A. R. Masri[a], G. Neuber[c], O. T. Stein[c], A. Kronenburg[c], A. Varna[d], E. R. Hawkes[d], B. Sundaram[e], A. Y. Klimenko[e], Y. Ge[f]

[a]*School of Aerospace, Mechanical and Mechatronics Engineering, The University of Sydney*
[b]*School of Engineering, Macquarie University*
[c]*Institut für Technische Verbrennung, Universität Stuttgart*
[d]*School of Mechanical Engineering, The University of New South Wales*
[e]*School of Mechanical and Mining Engineering, The University of Queensland*
[f]*Institut für Thermodynamik, Universität der Bundeswehr München*

Abstract

Computational models for combustion must account for complex and inherently interconnected physical processes including dispersion, mixing, chemical reactions, particulate nucleation and growth and, critically, the interactions of these with turbulence. The development of affordable and accurate models that are widely applicable is a work in progress. Stochastic multiple mapping conditioning (MMC) is a fast-emerging approach that has been successfully applied to non-premixed, premixed and partially premixed flames as well to the modelling of liquid and solid particulate synthesis. The method solves the conventional PDF transport equation but incorporates an additional constraint in that the mixing is localised in a reference space. This paper describes the numerical implementation of stochastic MMC in an OpenFOAM compatible code called mmcFoam. The model concepts and equations along with alternative submodels, code structure and numerical schemes are explained. A focus is placed on validation of the computational methods in particular demonstrating numerical convergence and mass consistency of the hybrid Eulerian/Lagrangian

*Corresponding author
Email address: m.cleary@sydney.edu.au (M. J. Cleary)

schemes. Four validation cases are selected including a combustion direct numerical simulation (DNS) case, two combustion experimental jet flame cases and a non-combusting particulate synthesis case. The results show that the total mass and mass distribution of Eulerian and Lagrangian schemes are consistent and confirm that the solutions numerically converge with increasing number of stochastic computational particles and sections for describing particulate size distribution.

Keywords: multiple mapping conditioning, MMC-LES, MMC-RANS, OpenFOAM, mmcFoam

1. Introduction

Practical combustion systems feature strongly non-linear interactions of turbulent motions with small-scale processes including chemical reactions, radiation and aerosol formation. Affordable computational models which apply filtering or averaging techniques to the governing equations have unclosed source terms and various turbulence-chemistry interaction (TCI) models are the subject of intensive research [1]. TCI models may be broadly divided into flamelet-like models [2] and transported probability density function (PDF) models [3]. The former, which include the fundamentally rigorous conditional moment closure (CMC) [4], parameterise the TCI in terms of one or more key quantities called conditioning variables. Such models are economical and provide a good resolution in the conditioning variable space to obtain a closure for the non-linear sources, but flamelet-like models are formally or practically restricted to specific combustion regimes. PDF models are more general since filtering or averaging is not applied to the sources which consequently appear in the transport equations as naturally closed terms. The PDF transport equation is highly dimensional and the most economical solution method involves a stochastic Monte Carlo simulation utilising an ensemble of Lagrangian particles [5]; lately referred to as *Pope particles* [6]. The traditional perspective is that PDF methods are more accurate but considerably more computationally expensive than alternative TCI models. In principle, PDF methods may be applied to non-premixed, premixed and mixed-mode combustion regimes. However, a difficulty arises with the modelling of molecular mixing which controls the dissipation of scalar variances and is unclosed in the PDF transport equation. Various mixing models have been developed over the years but none may yet be applied universally to all combustion regimes [7].

The multiple mapping conditioning (MMC) combustion model is a logical extension of the CMC and PDF methods [8], combining their attributes to reduce regime dependence and improve computational efficiency. The stochastic version of MMC, which is the focus of the present work, is a full PDF method in

which MMC plays the role of a mixing model that incorporates the conditioning ideas from the flamelet-like approaches. Since real mixing occurs by molecular motion between fluid elements which are local to each other in composition space, it is desirable that the mixing model should emulate this [9]. MMC achieves localness through use of a reference space. The concept is simple to implement. In addition to the thermodynamic and composition variables, each Pope particle also carries information about the evolving reference space. Prior to mixing, the particles are ordered in that reference space and the mixing interactions occur between pairs or groups of particles which are adjacent or close to each other in that ordered list. Any combination and type of reference variable is permitted [10] but in practice only a small number of reference variables is needed. For example, in non-premixed combustion the reference space may be mapped to the mixture fraction ensuring that excessive mixing does not occur across the stoichiometric contour which would lead to an overprediction of flame extinction. The mapping is statistical in that the reference variables and the quantities to which they are mapped describe the same statistical distribution but they are stochastically independent [11]. This indirect localness is essential otherwise the model would violate the mixing model linearity and independence principles [9] leading to deficiencies such as *stranding* and an underprediction of conditional variances [12].

In the original derivation of MMC [8] the reference variables were modelled as Markov diffusion processes, and this is the version commonly employed in the context of the Reynolds averaged Navier-Stokes form of the model (MMC-RANS) [13]. Later, generalised interpretations of MMC evolved [10, 14] which relaxed the Markov requirement and formulated alternative reference variable types including traced quantities from large eddy simulations (MMC-LES). PDF approaches in LES, called filtered density function (FDF) models [15], are conventionally implemented with a large number of Pope particles inside each LES grid cell to model the subgrid composition. These are called *intensive* or *dense* particle methods. In MMC-LES localness may be enforced in the reference space even if there are far fewer Pope particles than LES grid cells [16, 17]. These

sparse particle methods offer a significant computational saving, especially if complex chemical kinetics are involved.

An advanced C++ package called mmcFoam has been developed jointly by the authors of this paper. The code is compatible with the OpenFOAM suite of libraries [18] and incorporates both MMC-LES and MMC-RANS solvers with both sparse and intensive particle methods using various formulations of reference variables. Complex physics, including mixing, reaction and particle synthesis, and robust numerical schemes, including alternative chemical integrators, are implemented using a hierarchical and nested template structure and submodel classes. mmcFoam predictions have been compared to various detailed experimental [19, 20, 21, 22, 23] and DNS [17, 24] databases.

The main contribution of the present paper is to provide a thorough description and validation of the computational methods employed in mmcFoam. Section 2 presents the stochastic MMC model including details of a novel *Kernel Esimation* algorithm for coupling the hybrid Eulerian and Lagrangian representations of the turbulent fields. Section 3 describes the hierarchical code structure that uses template layers to facilitate the flexible inclusion of relevant aspects of turbulence, combustion and aerosol formation physics to suit specific simulation cases. The fine details of each layer, including information on numerical schemes, are contained in Appendix A. Section 4 contains a set of four test cases designed to validate the numerical methods with a focus on demonstrating (i) mass consistency between the hybrid finite-volume and stochastic-particle schemes, and (ii) numerical convergence with increasing number of stochastic particles and increasing number of aerosol number-density sections. Conclusions are found in Section 5.

2. The stochastic MMC model

A hybrid Eulerian and Lagrangian method is employed. The conservation of mass and momentum are modelled in Eulerian fashion and for this purpose mmcFoam links to the well-documented LES and RANS finite volume solvers

and turbulence models that are available in OpenFOAM [25]. The turbulent composition field is modelled in stochastic form with a Lagrangian Monte Carlo technique. Full derivations of the MMC-LES and MMC-RANS governing equations may be found in [26] and [23], respectively, and are not repeated here.

2.1. General form of the model

The composition field is $\boldsymbol{\phi} = (\boldsymbol{Y}, \boldsymbol{N}, h)$ where $\boldsymbol{Y} = (Y_1, ..., Y_{n_s})$ are the mass fractions of the transported molecular species, $\boldsymbol{N} = (N_1, ..., N_{n_d})$ are the number densities of the transported discrete particulate quantities and h is the standardised enthalpy. The modelling of number density follows a nodal sectional approach [22] and n_d is the number of nodes. For the purpose of the non-premixed combustion discussion below, a mixture fraction $Z = g(\boldsymbol{Y})$ is defined as the mass fraction of the composition originating in the fuel stream. It is a linear function of the composition variables and therefore evolves according to the same transport equations as $\boldsymbol{\phi}$. To assist the simulation of $\boldsymbol{\phi}$ a reference space $\boldsymbol{\xi} = (\xi_1, ..., \xi_{n_r})$ is also defined.

The turbulent composition is represented discretely on an ensemble of N_p Pope particles, each having a time dependent location, $\boldsymbol{x}^p(t)$, composition, $\boldsymbol{\phi}^p(t)$, and reference value, $\boldsymbol{\xi}^p(t)$. The first two evolve as [3, 7]

$$\mathrm{d}x_i^p = \left[\widetilde{u}_i + \frac{1}{\langle\rho\rangle}\frac{\partial}{\partial x_i}\left(\langle\rho\rangle\mathcal{D}_{\mathrm{eff}}\right)\right]^p \mathrm{d}t + \left[\sqrt{2\mathcal{D}_{\mathrm{eff}}}\right]^p \mathrm{d}\omega_i, \tag{1}$$

$$\mathrm{d}\phi_\alpha^p = [W_\alpha^p + S_\alpha^p]\,\mathrm{d}t. \tag{2}$$

Here, $\widetilde{\cdot}$ and $\langle\cdot\rangle$ denote quantities, respectively, which have been Favre and conventionally filtered (in the case of LES) or averaged (in the case RANS), u_i is the velocity in coordinate i, ρ is density, $\mathcal{D}_{\mathrm{eff}} = \mathcal{D}_m + \mathcal{D}_t$ is the effective diffusivity with molecular and turbulent components and $\mathrm{d}\omega$ is the increment of an independent Wiener process. Eq. (2) accounts for changes in composition variable α due to the source term, W, and molecular mixing, S. The former is the rate of chemical reactions, or aerosol nucleation and growth, or heat loss due

to radiation. Since expressions for these are known (e.g. Arrhenius expressions) W is in closed form. A mixing model is required for S. Subramaniam and Pope [9] outline desirable characteristics of mixing models and chief among them is the requirement that the mixing conserves the positionally local mean values of the composition. This constraint on the mixing operation can be expressed symbolically as $\langle S_\alpha | \boldsymbol{X} \rangle = 0$ where the mean is taken by summation over all particles in the ensemble on the condition that the quantity to the right of the vertical line is constant. The upper case $\boldsymbol{X}$ is the sample space for particle position, that is, a particular value in the range of $\boldsymbol{x}$. Other requirements of mixing [9] are that it should be local in composition space, and be both linear and independent with respect to the composition values. These dual qualities are achieved in MMC through an extension of the above constraint, viz:

$$\langle S_\alpha | \boldsymbol{\Xi}, \boldsymbol{X} \rangle = 0. \tag{3}$$

which expresses that MMC mixing conserves mean values locally in both the reference and position spaces. Note that $\boldsymbol{\Xi}$ is the sample space for $\boldsymbol{\xi}$. To satisfy the linearity and independence properties the reference space is strictly mathematically independent of composition space, but at the same time it must emulate the Lagrangian properties of the composition so that mixing which is local in $\boldsymbol{\xi}$-space is in fact also local in $\boldsymbol{\phi}$-space. In stochastic form the effect of mixing on the composition of a Pope particle may be written as

$$\mathrm{d}\phi^p_{\alpha,\mathrm{mix}} = -\frac{1}{\tau_L} \left(\phi^p_\alpha - \langle \phi_\alpha | \boldsymbol{\Xi}, \boldsymbol{X} \rangle \right) dt, \tag{4}$$

where τ_L is a mixing time scale. Estimating the conditional mean as [23]

$$\langle \phi_\alpha | \boldsymbol{\Xi}, \boldsymbol{X} \rangle^{p,q} = \frac{m^p \phi^p_\alpha + m^q \phi^q_\alpha}{m^p + m^q}, \tag{5}$$

where q is the nearest particle to p in $(\boldsymbol{\xi}, \boldsymbol{x})$-space and m represent the mass of a Pope particle, and then integrating Eq. (4) over a time step of Δt, leads to

the following variation in the compositions of both p and q:

$$\phi_\alpha^p\left(t+\Delta t\right) = \phi_\alpha^p\left(t\right)+\gamma\left(\langle\phi_\alpha|\boldsymbol{\Xi},\boldsymbol{X}\rangle^{p,q}-\phi_\alpha^p\right), \tag{6}$$

$$\phi_\alpha^q\left(t+\Delta t\right) = \phi_\alpha^q\left(t\right)+\gamma\left(\langle\phi_\alpha|\boldsymbol{\Xi},\boldsymbol{X}\rangle^{p,q}-\phi_\alpha^q\right). \tag{7}$$

Here

$$\gamma = 1-\exp\left(-\frac{\Delta t}{\tau_L^{p,q}}\right), \tag{8}$$

is the mixing extent that is determined locally and instantaneously for each pair of mixing particles.

In principle any number and type of reference variables can be used and mmcFoam has been structured for this purpose. For the non-premixed combustion conditions presented here only a single reference variable is used. We set $n_r = 1$ and $\boldsymbol{\xi} = f$ where f is a mixture fraction that is stochastically independent of Z but emulates its statistics through a mapping. Below we present separate details of the mapping for MMC-LES and MMC-RANS.

2.2. MMC-LES

In MMC-LES the reference mixture fraction is obtained by interpolation from the Eulerian LES field with $f^p(t) = f\left(\boldsymbol{x}^p,t\right)$ and, in general, $f\left(\boldsymbol{x},t\right) = \widetilde{f}\left(\boldsymbol{x},t\right)+f'\left(\boldsymbol{x},t\right)$ has filtered and subfilter components. Prior to mixing, the Pope particles are formed into pairs that are selected by minimising[1] the effective square distance between them in $(f,\boldsymbol{x})$-space,

$$\hat{d}_{p,q}^2 = \sum_{i=1}^{3}\left(\frac{d_{x_i}^{p,q}}{r_m/\sqrt{3}}\right)^2+\left(\frac{d_f^{p,q}}{f_m}\right)^2. \tag{9}$$

Here, r_m and f_m are model input parameters representing the characteristic distances between mixing particles in position and reference mixture fraction spaces, respectively, and $d_{x_i}^{p,q} = |x_i^p - x_i^q|$ and $d_f^{p,q} = |f^p - f^q|$ are the actual

[1] In mmcFoam this operation is performed through an efficient simplification of the k-d tree algorithm [27].

distances that are obtained after the minimisation. Cleary and Klimenko [26] formulated a simple algebraic relationship between r_m and f_m reducing it to a single parameter problem. It has been found that $f_m = 0.03$ works well in attached jet flames [28, 20] while somewhat higher values may be needed in some autoigniting lifted flames [19].

Two different models for τ_L have been developed for MMC-LES. The model first suggested in Ref. [26]

$$\tau_L^{p,q} = C_L^{-1} \frac{\beta C_f \left(d_f^{p,q}\right)^2}{2\mathcal{D}_{\text{eff}} \nabla \widetilde{f} \cdot \nabla \widetilde{f}}, \tag{10}$$

has been used in most MMC-LES simulations of practical flames. Here, $C_L = 1$, $C_f = 0.1$ and $\beta = 3$ are model constants. A new model which takes a more rigorous anisotropic view of the turbulent structures at the subfilter scale was recently suggested by Vo et al. [17]:

$$\tau_L^{p,q} = C_L^{-1} \frac{C_f \left(d_x^{p,q}\right)^2}{2\mathcal{D}_{\text{eff}}^*}, \tag{11}$$

Here, $\mathcal{D}_{\text{eff}}^* = \mathcal{D}_m + d_x^{p,q}/\Delta_E \mathcal{D}_t$. Detailed comparison of this anisotropic model against the older model for DNS of a reacting mixing layer found that the sensitivity of simulations to variations in f_m is diminished.

Since there are considerably fewer Pope particles than LES grid cells in sparse MMC-LES then $r_m > \Delta_E$; usually by a factor of two or three [26, 17]. At this scale the filtered component is the leading order term in evaluating $d_f^{p,q} = |f^p - f^q|$ and therefore it is usual to omit the subfilter component so that we set $f^p(t) \simeq \widetilde{f}(\boldsymbol{x}^p, t)$. The LES modelling of the filtered field $\widetilde{f}$ is conventional and given by

$$\frac{\partial \langle\rho\rangle \widetilde{f}}{\partial t} + \frac{\partial \langle\rho\rangle \widetilde{u}_i \widetilde{f}}{\partial x_i} - \frac{\partial}{\partial x_i}\left(\langle\rho\rangle \mathcal{D}_{\text{eff}} \frac{\partial \widetilde{f}}{\partial x_i}\right) = 0. \tag{12}$$

2.3. MMC-RANS

The modelling of f is different in the RANS setting due to the need to model all turbulent scales. Following Varna et al. [23] (but with different notation) it

is modelled stochastically as

$$\mathrm{d}f^p = -\frac{C_\phi}{\tau}\left(f^p - \tilde{f}\right)\mathrm{d}t + b_o\sqrt{\frac{2C_\phi\widetilde{f'^2}}{\tau}}\mathrm{d}\omega_f, \tag{13}$$

where, now, $\tilde{f}$ and $\widetilde{f'^2}$ are the Favre mean and variance of f that are estimated by summation over the dense Pope particle ensemble within a RANS cell, ω_f is another independent Wiener process, and C_ϕ and b_o are model constants. τ is the turbulence time scale and is modelled here as k/ε although alternatives are possible depending on the specific form of the RANS model that is chosen. MMC-RANS is a dense particle method and particle mixing pairs are selected from the same RANS grid cell on the condition that they are adjacent to each other in f-space. Once selected the particles mix according to Eq. (6) and (7) where $\tau_L = \tau/C_{\min}$ and $C_{\min}$ is the minor mixing constant.

The constant C_ϕ controls the rate of decay of $\widetilde{f'^2}$ and in-line with observations of mixture fraction in both experimental and DNS cases is commonly set to $C_\phi = 2$. For fixed C_ϕ the remaining MMC-RANS models constants, b_o and $C_{\min}$, control the mapping between f and Z. Varna et al. [23] selected them such that f and Z have approximately the same mean and variance[2]; $\widetilde{f} \approx \widetilde{Z}$ and $\widetilde{f'^2} \approx \widetilde{Z'^2}$. Different values of the constants are obtained for different flow conditions and in homogeneous turbulence they are

$$b_0 = \sqrt{1/2}, \tag{14}$$

$$C_{\min} = \frac{C_\phi}{2\left(1 - r_t^2\right)}, \tag{15}$$

where r_t is a target correlation function between f and Z. For r_t close to unity these settings for b_0 and $C_{\min}$ also work well in inhomogeneous flows and it was subsequently shown that $r_t = 0.935$ produces good predictions for both reactive and non-reactive scalars in jet diffusion flames [29].

[2]Although the first two moments are similar, their PDF's differ somewhat, most notably by the fact that f is unbounded while $Z \in [0, 1]$

2.4. Coupling of the Eulerian and Lagrangian models

The stochastic equations (1) and (2) are a model for the filtered (LES) or averaged (RANS) mass density function. Defining the discrete mass density function as

$$F^{*}\left(\boldsymbol{\Phi},\boldsymbol{X};t\right)=\sum_{p=1}^{N_p} m^{p}\delta\left(\boldsymbol{\Phi}-\boldsymbol{\phi}^{p}(t)\right)\delta\left(\boldsymbol{X}-\boldsymbol{x}^{p}(t)\right), \tag{16}$$

where, as before, the uppercase symbols are the sample space variables, and $\delta\left(\boldsymbol{\Phi}-\boldsymbol{\phi}^{p}(t)\right)$ and $\delta\left(\boldsymbol{X}-\boldsymbol{x}^{p}(t)\right)$ are multidimensional delta functions, the continuous mass density function is then obtained by taking the conventional filter or average:

$$\left\langle F^{*}\left(\boldsymbol{\Phi},\boldsymbol{X};t\right)\right\rangle = F\left(\boldsymbol{\Phi};\boldsymbol{x},t\right). \tag{17}$$

In conjunction with the continuity and Navier-Stokes equations the model for F describes the thermodynamic state of the turbulent flow. Consistency between the Lagrangian and Eulerian representations requires that $\sum_{p=1}^{N_p} m^{p} = m_t$, where m_t is the total mass in the system, and that the spatial distribution of the Lagrangian mass matches that of the continuum fluid mass distribution. These dual requirements are achieved by a combination of (i) consistent definitions of Lagrangian and Eulerian fields at initialisation and at the boundaries, and (ii) accurate two-way coupling of the fields as described next.

The Eulerian LES or RANS field, computed on a finite volume grid, provides the Lagrangian field, computed on the Pope particles, with velocity, density, turbulent diffusivity and, in the case of LES, reference mixture fraction. In turn, the Lagrangian field provides the density (a function of $\boldsymbol{\phi}$, pressure and the equation of state) back to the Eulerian field. The density feedback from the discontinuous Lagrangian field to the continuous Eulerian field requires special treatment to avoid numerical instability that can be acute in sparse MMC-LES simulations where some grid cells do not contain any Pope particles. In mmcFoam an adaptation of the equivalent enthalpy concept [30] is used. Additional Eulerian transport equations are solved for the composition. The real (and statistically correct) composition is modelled on the Pope particles and, to dif-

ferentiate it, the Eulerian composition is described as an *equivalent composition* field and given the notation ϕ^E. From ϕ^E the Eulerian density is then obtained through the pressure and the equation of state. The transport equation for filtered or averaged equivalent composition is

$$\frac{\partial\langle\rho\rangle\widetilde{\phi_\alpha^E}}{\partial t}+\frac{\partial\langle\rho\rangle\widetilde{u}_i\widetilde{\phi_\alpha^E}}{\partial x_i}-\frac{\partial}{\partial x_i}\left(\langle\rho\rangle\mathcal{D}_{\text{eff}}\frac{\partial\widetilde{\phi_\alpha^E}}{\partial x_i}\right)=\widetilde{W}_\alpha^E. \tag{18}$$

The influence of the Lagrangian composition field is restricted to the source term which is modelled as [26]

$$\widetilde{W}_{\phi_\alpha}^E=\langle\rho\rangle\frac{\widetilde{\phi_\alpha^E|\boldsymbol{\phi}_{\boldsymbol{c}}^{\boldsymbol{E}}}-\widetilde{\phi_\alpha^E}}{\tau_{rel}}. \tag{19}$$

where $\widetilde{\phi_\alpha^E|\boldsymbol{\phi}_{\boldsymbol{c}}^{\boldsymbol{E}}}$ is the Favre mean of equivalent species α conditional on a particular value of the set of coupling equivalent species $\boldsymbol{\phi}_{\boldsymbol{c}}^{\boldsymbol{E}}$. In general, $\boldsymbol{\phi}_{\boldsymbol{c}}^{\boldsymbol{E}}$ is used for different purposes than the reference space, $\boldsymbol{\xi}$, and the two may be computed independently or they may share some elements. For example as explained in Ref. [26] in MMC-LES of non-premixed combustion we have both $\boldsymbol{\xi}=\widetilde{f}$ and $\boldsymbol{\phi}_{\boldsymbol{c}}^{\boldsymbol{E}}=\widetilde{f}$ but other combustion modes and versions of the MMC model will require alternative treatments. In Eq. (19) $\tau_{rel}=K\Delta t$ is a relaxation time scale and $K\sim 10$ has been found to produce smooth $\widetilde{\phi^E}$ fields in most circumstances. The source is not stiff and the equivalent composition simulation does not add a significant computational cost. An estimation of the conditional mean $\widetilde{\phi_\alpha^E|\boldsymbol{\phi}_{\boldsymbol{c}}^{\boldsymbol{E}}}$ is requierd and two different approaches are possible which constitute two different submodels in mmcFoam. These are called `FlameletCurves`[3], which is based on sparse MMC-LES coupling method suggested in Ref. [26], and `KernelEstimation` which is based on ideas developed in the field of smoothed particle hydrodynamics (SPH) [31].

The `FlameletCurves` submodel involves a pre-processing step to compute a table of flamelet-like curves for species mass fractions and sensible enthalpy

[3]To enhance readability, a different font is used to distinguish code elements such as `code blocks`, `templates`, `classes` and `objects`.

as a function of the coupling equivalent species, $\boldsymbol{\phi_c^E}$. Then during the simulation a parametric regression is performed which aims to find the flamelet curve that best matches the conditionally averaged composition of the Pope particle ensemble in the spatial region around each LES cell. That region is defined by multiple LES or RANS cells (typically four or five) in each coordinate direction. Once the flamelet curve is selected, the value of $\widetilde{\phi_\alpha^E|\boldsymbol{\phi_c^E}}$ in the LES or RANS cell is approximated from the flamelet curve using the Eulerian value $\boldsymbol{\phi_c^E}$ as the input parameter.

The `KernelEstimation` submodel does not require pre-computed flamelet tables but instead estimates $\widetilde{\phi_\alpha^E|\boldsymbol{\phi_c^E}}$ by a radial basis function

$$\widetilde{\phi_\alpha^E|\boldsymbol{\phi_c^E}} = \int_{-\infty}^{\infty} \phi_\alpha^E(\mathbf{r}')\Omega(\mathbf{r}-\mathbf{r}',\boldsymbol{\Delta})d\mathbf{r}', \tag{20}$$

where Ω is a kernel function (units of m^{-3}) and $d\mathbf{r}'$ indicates integration over $\left(\boldsymbol{\phi_c^E},\boldsymbol{x}\right)$-space. The interpolation exactly reproduces the scalar value ϕ_α^E if the kernel is a Delta function which would imply a resolution length scale of $\Delta = 0$. However, the composition values are known only at discrete locations and the number of Pope particles is finite. Therefore integral interpolation is approximated by a summation over the entire ensemble,

$$\widetilde{\phi_\alpha^E|\boldsymbol{\phi_c^E}} \simeq \sum_p m^p \frac{\phi_\alpha^p}{\rho^p}\Omega(\boldsymbol{r}-\boldsymbol{r}^p,\boldsymbol{\Delta}). \tag{21}$$

In dense simulations there are many particles in each Eulerian cell and the interpolation may be easily performed in physical space only with $\mathbf{r} = \{\boldsymbol{x}\}$ while the kernel is given by the convolution of linear basis functions with the length scale Δ equal to the LES or RANS cell size. In sparse simulations, the scalar variations in physical space may be large so we use $\mathbf{r} = \{\boldsymbol{\phi_c^E},\boldsymbol{x}\}$ and the kernel function is

$$\Omega(\mathbf{r}-\mathbf{r^p},\boldsymbol{\Delta}) = \prod_i \Omega_i(r_i - r_i^p,\Delta_i), \tag{22}$$

where the index i runs over each dimension of $\mathbf{r}$. For instance, in the mixture fraction based simulations presented where $\boldsymbol{\phi_c^E} = \widetilde{f}$ we have $\mathbf{r} = \{\tilde{f},\boldsymbol{x}\}$ at the

cell centres of the LES or RANS cell on which the equivalent species transport equation are being solved and $\mathbf{r^P} = \{\boldsymbol{x}^p, Z^p\}$ are the values on the Pope particles. In the present implementation, the characteristic length in conditional space, Δ_ξ, is fixed while the characteristic length scale in physical space, Δ_x is dynamically computed by an efficient search algorithm, such that in the limit their being infinite particles the kernel would reduce to a Delta function.

3. Numerical implementation

This section describes the hierarchical structure of mmcFoam which is an OpenFOAM-compatible C++ code that uses template layers to facilitate the flexible inclusion of relevant aspects of turbulence, combustion and aerosol formation physics to suit specific simulation cases. This structural flexibility is inherent to the architecture of OpenFOAM [18, 25] and the present implementation is a novel extension of that. Obviously the stochastic MMC theory and this numerical implementation could be coupled with other CFD solvers and the results presented in Section 4 therefore serve both as a validation of mmcFoam, specifically, and as a demonstration of mass consistency and numerical convergence in MMC-LES and MMC-RANS approaches, more generally.

mmcFoam is divided into two directories; `solvers` and pre-processing `utilities` are found in the `applications` directory, and core libraries are in the `src` directory. The `applications` are high-level code routines that initialise the objects and advance the fields in time by linking dynamically to the `src` libraries which contain all the detailed implementation of the numerical algorithms and the IO (input-output) code for reading and writing of data to file and parallel computing. Each of the `solvers` performs a very specific task. For example, the basic MMC solver deals with turbulent non-premixed combustion of gaseous fuels while others deal with turbulent multiphase, premixed and stratified combustion. The base solver is an extension of OpenFOAM's low-Mach compressible solver called `rhoPimpleFoam`.

The `src` is further divided into two blocks; the `mmc` block and the `mul-`

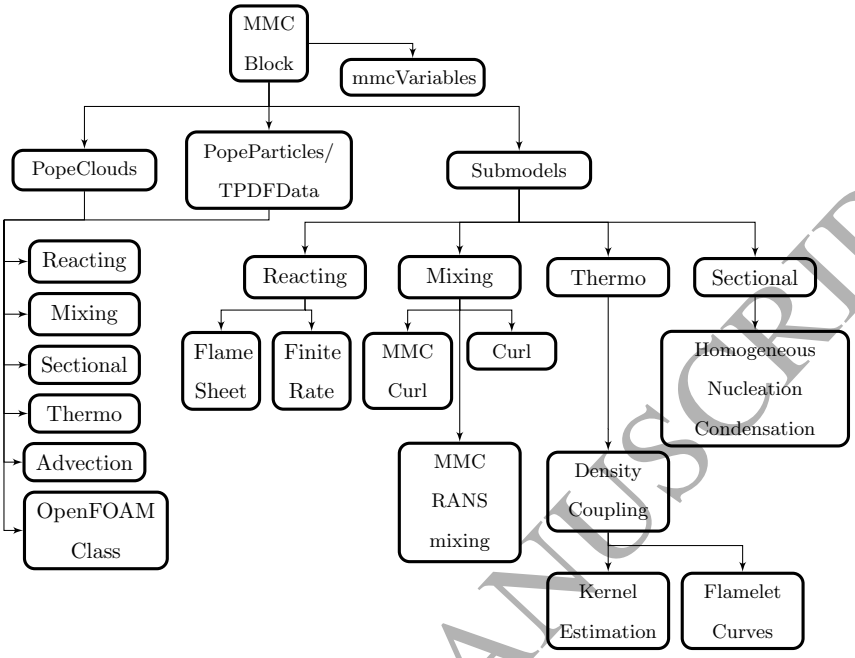

Figure 1: mmcFoam blocks

`tiphase` block. The latter deals with Lagrangian fuel particle tracking and interphase heat and mass transfer but it is not covered in the present paper. Figure 1 presents the structure of the `mmc` block. Template classes are used to segregate the different physical processes and at compile time they are nested together in different combinations to form derived classes with all the desired physical features of the model. The starting points for this architecture are the OpenFOAM `particle` and `cloud` classes. The `particle` class contains the basic variables and tools needed for Lagrangian modelling such as position. The `cloud` is a container class with the capability of adding and deleting particles. On top of these basic features the physics of the stochastic MMC model are added by nesting the template class layers with each layer being derived from and inheriting the properties of the preceding layer. The five layers (existing at the time of publication) are shown in Fig. 1. The `Advection` layer implements transport in physical space whereas the `Thermo`, `Sectional`, `Mixing`

and `Reacting` layers implement the evolution in scalar space. For the interested reader, specific details of the five layers, including information on the numerical schemes, are provided in Appendix A.

Encapsulation of the different physical processes within their own template class provides code security, which is useful in large collaborations such as this, and it also gives great flexibility. As can be seen in Fig. 1, each of these classes forms a layer that can be stacked by means of inheritance such that `PopeParticles` can be tailored to include the pieces relevant to the case studied. From a numerical point of view the multi-layer structure is akin to the fractional step method. Within the existing limits of the `mmc` code block, the most algorithmically complex case to model is turbulent combustion leading to aerosol formation. In such a case all the templates are required and a derived class is defined by the following combination:

$$\texttt{Reacting} \leftarrow \texttt{Mixing} \leftarrow \texttt{Sectional} \leftarrow \texttt{Thermo} \leftarrow \texttt{Advection} \leftarrow \texttt{particle}$$

Simpler combinations are also possible. For example, if modelling non-reacting scalar mixing the following combination may be used:

$$\texttt{Mixing} \leftarrow \texttt{Thermo} \leftarrow \texttt{Advection} \leftarrow \texttt{particle}$$

The simplest way to build up the capabilities of the derived `PopeParticles` classes would be in a series as shown on the left hand side of Fig. 2. However, this simplicity is complicated by the fact that there is interconnection between the physical processes. For example mixing affects gaseous chemical species, which are data members in the `Thermo` template class, and it also affects the number density of small synthesised particulates, which are data members in the `Sectional` template class. Moreover, each of the template classes have their own supporting member data which are essential for computational purposes but that are not transported elements of the composition space, $\boldsymbol{\phi}$. Temperature in the `Thermo` layer and interpolated velocity in the `Advection` layer are obvious examples. To handle this interconnnection an additional family of classes called `TPDFData` are defined concurrently with the

`PopeParticles` template classes. The `TPDFData` classes extract the transported variables from each layer and stack them together into an object on which the transport processes are applied. This hub-and-spoke type of architecture is shown schematically on the right hand side of Fig. 2.

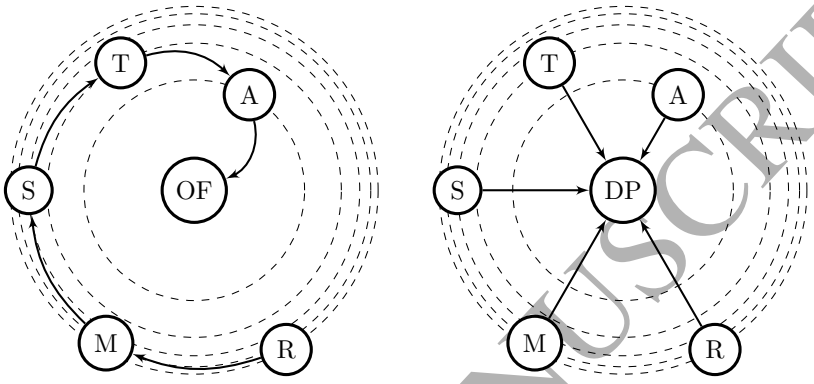

Figure 2: Concept depiction of PopeParticle (left) and TPDFData (right). R: reaction, M: mixing, S: Sectional, T: Thermo, A: Advection, OF: OpenFOAM Particle, DP: TPDFData Particle.

Two final aspects of the code structure shown in Fig. 1 remain to be discussed. The first is the `Submodels` which are abstract classes designed to incorporate alternative runtime selectable physical models for each of the template class layers. The implementation follows that found in the main OpenFOAM code and the details of the existing mmcFoam submodels are discussed in Appendix A. The second aspect is the `mmcVariables` which is a generic class platform that controls the purpose of the chosen reference variables, $\boldsymbol{\xi}$, and coupling variables, $\boldsymbol{\phi_c^E}$. Different weightings may be applied to each of the reference and coupling variables and the best choice of these weightings depends strongly on the combustion mode. For non-premixed combustion the mixture fraction is a suitable quantity for both localisation and density coupling and it is simplest, but not compulsory, to choose the same weighting for the mixture fraction in both operations while the weighting for other scalar quantities is zero. Alternatively it would be possible to use a shadow position reference

variable [32] to localise the mixing operation while choosing the mixture fraction or progress variable for the density coupling in non-premixed and premixed combustion, respectively. In that case the mixture fraction or progress variable could be given a zero-weighting for localisation and the shadow position could be given a zero-weighting for density coupling. Furthermore, the `mmcVariables` class controls whether the reference variables are obtained by interpolation of an Eulerian reference field to the particle location, as is done MMC-LES, or by solving stochastic equations, as is done for MMC-RANS.

4. Validation

The MMC-LES and MMC-RANS computational models in mmcFoam have been tested against various experimental [19, 20, 21, 22, 29] and DNS [17] databases previously. The contribution of the present paper is to validate the numerical implementation with a focus on mass consistency between the Eulerian and Lagrangian schemes and numerical convergence with respect to the number of Pope particles and synthesised particulate sections used in the stochastic simulations. Mass consistency analysis of MMC-LES is conducted in Sec. 4.1 for simulations of the Sydney piloted burner with inhomogeneous inlets [33] that was previously used to test MMC-LES predictions of mixed-mode combustion [20]. Recently, numerical convergence of MMC-LES was studied against DNS data of a syngas shear layer [17] and the most pertinent aspects of this, along with some new results, are discussed in Sec. 4.2. This is followed by numerical analysis of two further experimental test cases. The first, Sandia flame D, is a piloted methane/air jet diffusion flame [34] which was previously modelled in [23]. In Sec. 4.3 the case is used to explore numerical convergence of MMC-RANS. Finally, in Sec. 4.4 MMC-LES numerical convergence with respect to the number of Pope particles and the number of particulate sections is investigated for the Lesniewski and Friedlander experimental configuration [35] of dibutyl-phthalate (DBP) condensation and growth in a heated nitrogen jet. This case was previously modelled in [22]. A summary of the test cases and

model settings, specifically submodel selection, can be found in Table 1.

Table 1: mmcFoam validation cases. FS: `FreeStream`, KE: `KernelEstimation`, FC: `FlameletCurves`, oTR: `opticallyThinRadiation` MC: `MMCCurl`, HNC: `Homogeneous-NucleationCondensation`, fRPR: `finiteRateParticleReaction`. Section 2.4 contains full descriptions of the KE and FC submodels, while the basic elements of the other submodels can be found in Appendix A.

Case	inhomogeneous inlet burner	shear layer	Sandia Flame D	condensing DBP jet
Type	Exp.	DNS.	Exp.	Exp.
Fuel	CH_4/air	syngas	CH_4/air	DBP/N_2
Ref.	[33, 20]	[17]	[34, 29]	[35, 22]
Method	MMC-LES sparse	MMC-LES sparse	MMC-RANS dense	MMC-LES sparse
Advection	FS	FS	FS	FS
Thermo	KE / FC oTR	none	KE oTR	none
Mixing	MC	MC	MC	MC
Sectional	none	none	none	HNC
Reacting	fRPR	fRPR	fRPR	none

4.1. Inhomogeneous inlet burner: demonstration of mass consistency in MMC-LES

Mass consistency between the coupled Eulerian and Lagrangian representations of the turbulent fields requires that the two fields have equivalent initial and boundary conditions, that Pope particle number control algorithms are mass conservative and that an accurate density coupling scheme is employed. Here we concentrate on the last of these elements since its implementation is

Table 2: Experimental parameters for selected cases.

Flame	Lr (mm)	U_b (m/s)	U_{Air} (m/s)	U_{Fuel} (m/s)	Re
H	300	59	61.5	69.2	27600
I	75	80	83.4	93.8	37500

unique to mmcFoam while the other elements are standard [7].

Density coupling follows the adapted equivalent enthalpy method in which estimation of the conditional mean equivalent species, $\widetilde{\phi_\alpha^E|\boldsymbol{\phi}_{\boldsymbol{c}}^{\boldsymbol{E}}}$ in Eq. (19), is non-trivial. Two mmcFoam submodels called `FlameletCurves` and `KernelEstimation` are described in Section 2.4. The former method has been used in all past MMC-LES publications while the latter is a new approach that is used here for the first time.

The validation cases are two flames on the Sydney inhomogeneous inlet burner which is a relatively new experimental platform for investigating multi-mode combustion [33]. The flames were previously simulated using the `FlameletCurves` density coupling approach [20]. The burner consists of two concentric tubes shrouded by a stoichiometric five gas pilot (5GP) stream of acetylene, hydrogen, oxygen, nitrogen and carbon dioxide. The inner tube can slide within the annulus so that for sufficiently large recess distances, Lr, the fuel/air mixture at the burner tip is near-homogeneous and for shorter Lr the mixture is compositionally inhomogeneous. The entire burner assembly is centred in a wind tunnel with a square cross section of 15x15 cm^2 which provides a uniform air co-flow at 15 m/s. In the present study methane fuel issues from the inner tube and air from the annulus with a volumetric air to fuel ratio of 2:1. Table 2 presents the main parameters for the two simulated cases; flame H with a near-homogeneous composition at the burner tip and flame I with an inhomogeneous mixture. In flame H a non-premixed flame structure forms throughout the field and in flame I a premixed flame structure forms near the burner and this transitions axially and radially to a non-premixed structure.

The computational domain consists of a 3D rectangular mesh that extends

$50D$ (jet diameters) axially and $10D$ in the lateral directions. The LES mesh has 1.4M cells and is refined in the jet and pilot regions resulting in a minimum mesh size of $\Delta_E = 0.4$ mm near the centreline. For the Lagrangian scheme there is 1 particle per 8 Eulerian LES cells (1L/8E). The standard Smagorinsky model and the reduced methane chemical mechanism DRM-22 [36] are used.

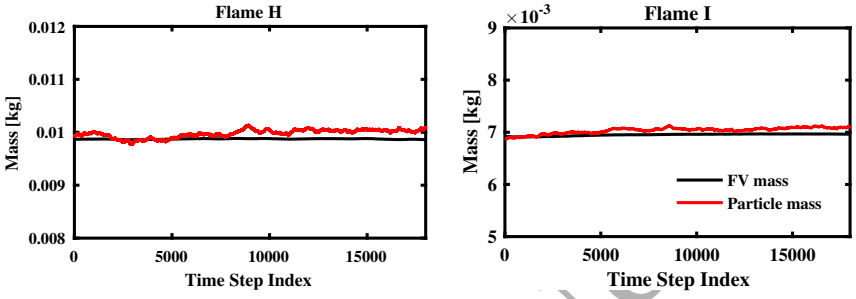

Figure 3: Total mass in the Eulerian (denoted FV mass) and Lagrangian (denoted Particle mass) computational domains versus time step for Flame H (left) and Flame I (right).

Figure 3 shows the total Eulerian and Lagrangian domain masses versus the time step index. The results are for simulations using the `KernelEstimation` method. The figures show that over the course of 20,000 time steps the mass of the two fields is in reasonable agreement, generally differing by less than a few percent. This relatively small difference reflects the fact that each has its own independent numerical schemes and equivalent although mathematically independent boundary conditions. The mass discrepancy has been found to diminish when the domain size increases due to reduced influence of the stochastic particle outflow boundaries.

Next the consistency of the mass distributions is investigated. In order for there to be consistent density distributions in the two fields the smoothed Lagrangian composition and the Eulerian equivalent composition must be similar. First we look at the temperature since it has the dominant effect on fluid density. Fig. 4 shows segments of the Eulerian equivalent temperature field, $\widetilde{T}^E$, for Flame H and the corresponding conditional temperature, $\widetilde{T^E|\boldsymbol{\phi}^{\boldsymbol{E}}_{\boldsymbol{c}}}$, that is obtained from the Pope particle ensemble. Each row represents a different in-

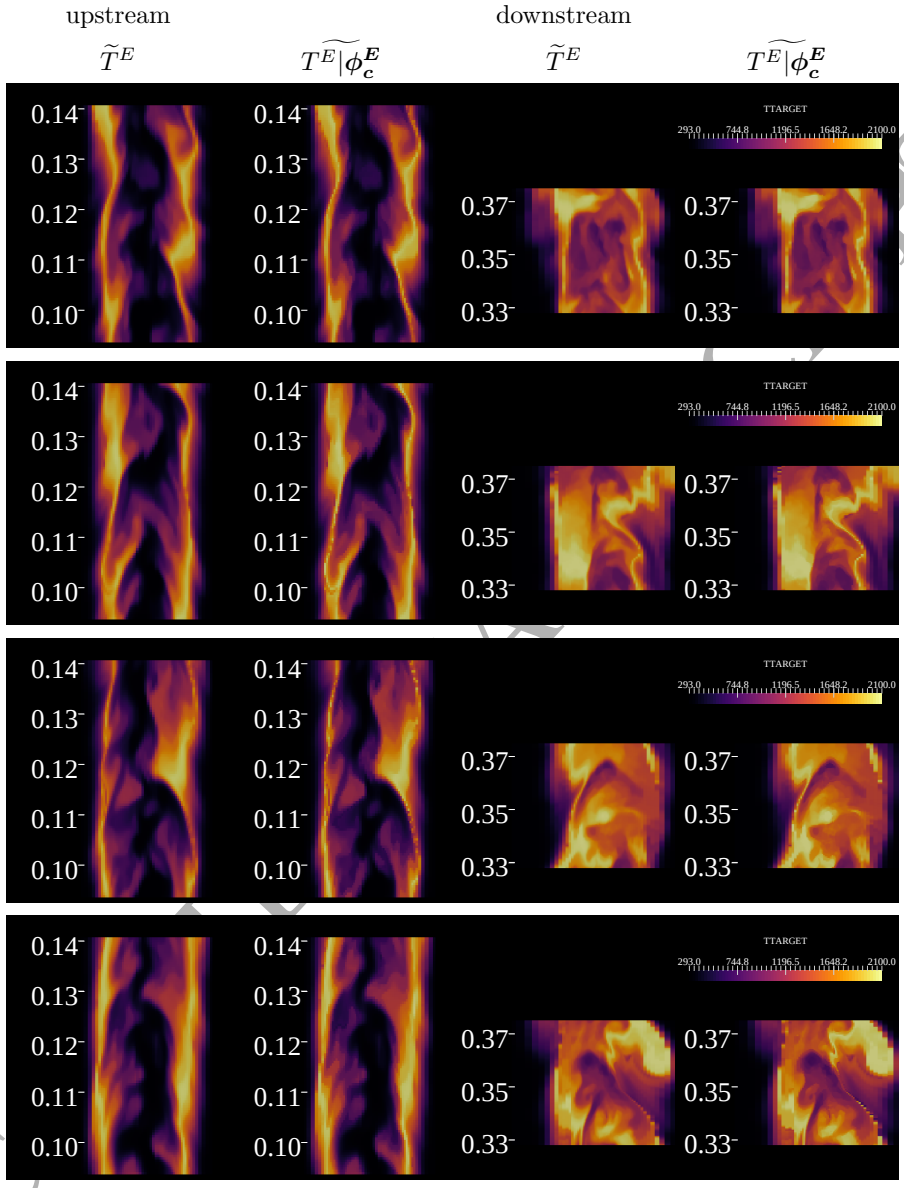

Figure 4: Equivalent temperature fields in Flame H at four different time steps (top to bottom) and two different axial zones. The upstream zone is from 0.09 m to 0.14 m above the burner and the downstream zone is from 0.33 m to 0.37 m above the burner. $\widetilde{T}^E$: Eulerian equivalent temperature given by Eq. (18), $T^{\widetilde{E|\phi_c^E}}$: smoothed Lagrangian temperature given by summation over the Pope particle ensemble according to Eq. (21).

stant in time and has upstream and downstream segments. Differences between the Eulerian and (smoothed) Lagrangian fields are almost imperceptible, giving an excellent account of the capacity of the `KernelEstimation` method to reconstruct a smooth three-dimensional composition field from a sparse set of particles.

Time sequences of scatter plots of Flame H hydrogen and carbon monoxide mass fractions versus the mixture fraction are presented in Fig. 5. To rigorously test the method a transient response is imposed on this sequence. A short time before $t = 0.01446$ s the fields were reinitialised with an equilibrium mixture of major combustion species (fuel, oxygen, nitrogen, carbon dioxide and water gas) while hydrogen and carbon monoxide were absent. As the finite rate chemistry calculated on the Pope particles ensues the two species are produced and reach a statistically steady state as may be seen in the progression from left to right. The `KernelEstimation` method attempts to produce a similar transient response for the Eulerian equivalent hydrogen and carbon monoxide mass fractions. The coupling correctly captures the transient variations and a consistent level of local flame extinction which produces the vertical scatter in the plots. As may be expected due to the numerically diffusive nature of finite volume solutions, the Eulerian data points have slightly more rounded profiles near the stoichiometric peaks but overall the consistency between the two fields is very good.

Finally, two MMC-LES simulations using the `FlameletCurves` and `KernelEstimation` methods are compared against each other and the experimental data. Radial profiles of Favre mean and RMS of temperature are presented in Figs. 6 for both Flames H and I. As expected for the non-premixed Flame H in which the filtered mixture fraction is a very suitable MMC-LES reference variable, there is a good agreement to the experimental data. The `FlameletCurves` and `KernelEstimation` approaches give very similar results. As explored in detail in Ref. [20], the agreement to the data for MMC-LES with a mixture fraction reference variable is not as good for Flame I as it was for Flame H. Additionally the results obtained with the `FlameletCurves` and `KernelEstimation` submodels exhibit greater differences than they do

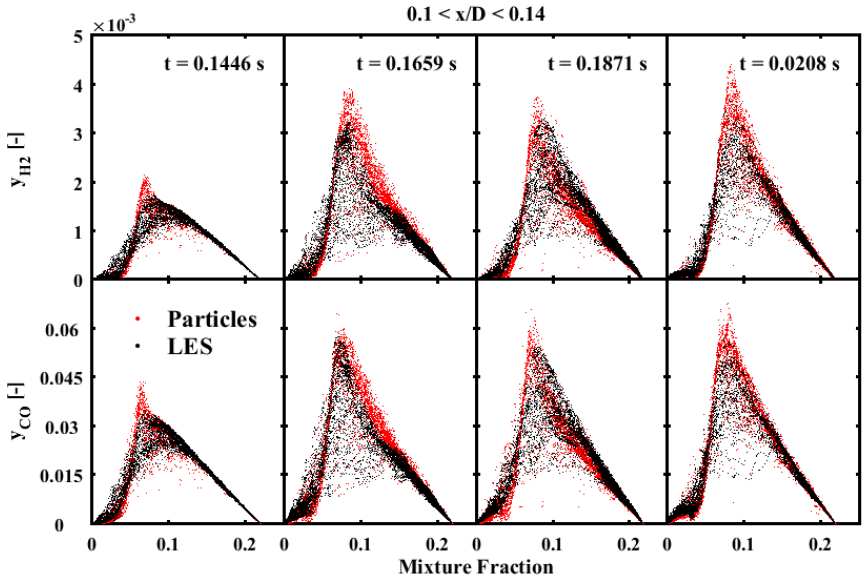

Figure 5: Scatter plots of species mass fraction versus mixture fraction in Flame H. Red dots are particle data, $\left(Z^p, \phi_\alpha^p\right)$, and black dots are equivalent species computed on the Eulerian grid, $(\widetilde{f}, \widetilde{Y_\alpha}^E)$. Data is obtained for locations from $0.1D$ to $0.4D$ downstream of the burner.

for Flame H. The compositional inhomogeneity at the burner tip and the ensuing premixed flame structure produces gradients of $\widetilde{\boldsymbol{\phi}^E|\boldsymbol{\phi}_{\boldsymbol{c}}^{\boldsymbol{E}}}$ in mixture fraction space that approach infinity (noting that, here, $\boldsymbol{\phi}_{\boldsymbol{c}}^{\boldsymbol{E}} = f$). In that region of the flame the `FlameletCurves` method results in rapid transition between different curves leading to excessive density fluctuations and numerical instability. To avoid instability the flamelet table entries with steep gradients in mixture fraction space (i.e. with premixed structures) are eliminated and consequently the method does not produce a consistent density distribution. The `KernelEstimation` method is much better in this respect since the kernel is weighted in both $\boldsymbol{x}$-space and f-space and the former dominates the evaluation of $\widetilde{\phi_\alpha^E|\boldsymbol{\phi}_{\boldsymbol{c}}^{\boldsymbol{E}}}$ when the mixture fraction gradient is very large permitting a smooth and consistent evaluation of the density field on the Eulerian mesh.

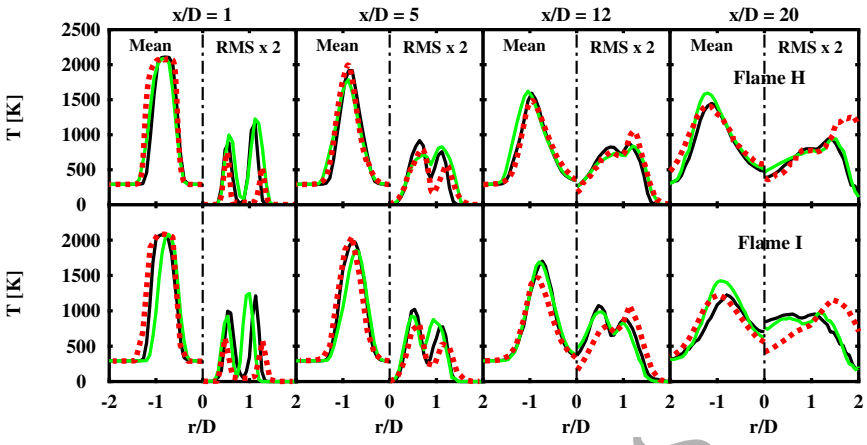

Figure 6: Radial profiles of mean and RMS of temperature for Flam H (first row) and Flame I (second row). Symbols - exp. data [33], black lines - MMC-LES using `FlameletCurves`, green lines - MMC-LES using `KernelEstimation`.

4.2. Syngas shear layer: demonstration of numerical convergence in MMC-LES

Ideally, stochastic MMC predictions should be independent of the number of Pope particles used in the simulations and should converge towards a unique model solution as $N_p \rightarrow \infty$. Furthermore, if the model is good then that numerically converged solution will converge to the exact solution for that flow. Being a hybrid method, there are a number of different length and filter scales in sparse MMC-LES to consider when devising a numerical convergence test. Δ_E is the filter width of the Eulerian LES fields and is typically equal to the mesh size. $\Delta_L \sim N_p^{-1/3}$ is the nominal distance between Pope particles irrespective of which particle mixing pairs are formed. Although it is a resolution scale that can be important for evaluation of statistical moments of the ensemble, it is not in itself a filtering scale. Filtering of the Lagrangian turbulent fields occurs through the mixing operation and the mean Lagrangian filter scale is therefore the mean value of $d_x^{p,q}$ in Eq. (9). Mixing is a stochastic process and for any one particle pair $d_x^{p,q}$ has a stochastic value while its expected value (denoted d_x) is controlled through the characteristic mixing distance r_m and this is a model input parameter linked to the characteristic mixing distance in

reference mixture fraction space, f_m. Among all these scales f_m is the only one requiring its value to be explicitly set and all the other scales are subsequently calculated from it. For a fixed set value f_m, taking the limits $N_p \to \infty$ and $\Delta_L \to 0$ leads to $r_m \to 0$ and subsequently $d_x \to 0$ as localisation in $\boldsymbol{x}$-space becomes dominant when attempting the minimisation of $\hat{d}^2_{p,q}$ in Eq. (9). This has a subsequent influence on the asymptotic behaviour of the mixing time scale. While the original model for τ_L given by Eq. (10) is independent of d_x, the recently developed anisotropic time scale model given by Eq. (11) leads to $\tau_L \to 0$ for $d_x \to 0$.

The above discussion illustrates a situation whereby an increase in the numerical parameter N_p can modify the model time scale τ_L and consequently the rate of dissipation of subfilter scalar variances. In general, the sensitivities towards model parameters and numerical parameters need to be investigated in isolation. Following Sundaram et al. [19] a different approach to the naive approach described in the preceding paragraph is chosen to demonstrate numerical convergence of the MMC-LES model whereby the limit $N_p \to \infty$ is approached in such a way that the model remains unchanged. For a fixed LES grid and a fixed value of the primary mixing model parameter f_m, a sparse base case is defined with $N_p = N_p^0$, $\Delta_L = \Delta_L^0 > \Delta_E$ and $r_m = r_m^0$. Numerical convergence is tested by increasing N_p in integer multiples, $N_p = i \cdot N_p^0$, and then at each mixing fractional step during the simulation the ensemble is randomly divided into i groups such that in each group there are N_p^0 particles, the nominal particle resolution is Δ_L^0 and the characteristic mixing distance is r_m^0. Mixing pairs are selected from each group in isolation so that in each group the expected mixing distance is $d_x = d_x^0$ which remains unchanged from the base case thus preserving the sparse nature of the mixing model despite there now being many more particles than LES grid cells.

Vo et al. [17] recently demonstrated numerical convergence following the scheme described above against the DNS solution of a combusting shear layer and here the most pertinent aspects of that study are reviewed followed by a couple of results from that case that were not previously published. The case

is a temporally evolving double shear layer with a syngas jet surrounded by counterflowing O_2/N_2 oxidiser. The domain is a rectangular prism of $L_x \times L_y \times L_z = 8.64 \times 10.065 \times 5.76$ mm^3 and the flow in it has a characteristic velocity $U = U_{fuel} - U_{oxidizer} = 145$ m/s from which the characteristic jet time is defined as $t_j \equiv H/U$ where $H = 0.72$ mm is the initial height of the syngas potential core. To study numerical convergence in isolation while eliminating decorrelation of the LES and DNS flows fields, spatial transport of the Pope particles is based *a posteriori* on the instantaneous DNS velocity and all subsequent quantities that are input to the MMC model are obtained from explicit spatial filtering of the DNS fields. The number of particles is varied in factors of eight over more than three orders of magnitude from 1 particle per every 8 LES cells, 1L/8E, to 128 particles per LES cell, 128L/1E, cf. Table 3. Although mixing pairs are selected to preserve the sparse nature of the model in the present convergence study, the number of particles used in the 1L/8E case is comparable to a typical sparse MMC-LES of an experimental flame case while the number used in the 128L/1E case is comparable to a typical dense PDF approach. The computational cost is proportional to the number of particles and this illustrates the great potential of sparse methods for practical applications, provided the predictions can be shown to numerically converge.

Table 3: Test cases for numerical convergence study. $f_m = 0.01$, $r_m = 1.46$ mm and $\Delta_E = 0.24$ mm are constant.

Case	N_p	Δ_L [mm]
1L/8E	4,536	0.47
1L/1E	36,288	0.24
32L/1E	1,161,216	0.0755
128L/1E	4,644,864	0.0476

Figure 7 shows mean d_x and d_f, obtained by averaging over the homogeneous flow directions (x and z), as functions the cross-stream coordinate y normalised

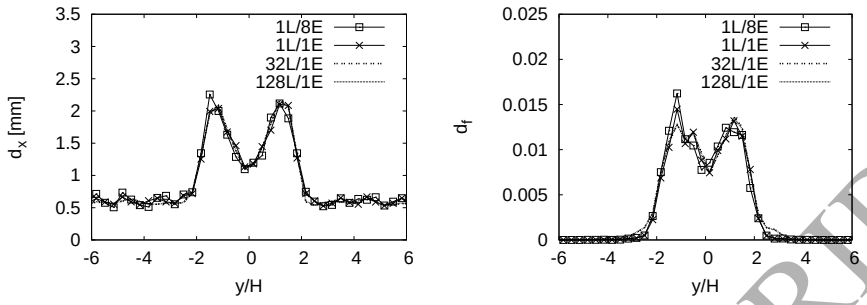

(a) (b)

Figure 7: Cross-stream profiles of (a) mean d_x, and (b) mean d_f at $t/t_j = 10$.

by the initial jet height H. It can be observed that the algorithm described above for mixing pair selection ensures that d_x and d_f remain effectively unchanged even when there are up to 128 particles per LES cell, thus ensuring τ_L is not affected by the number of particles and preserving the sparse nature of the mixing model (i.e. preserving $d_x > \Delta_E$). Also, the peak values of d_x and d_f in the shear layers reasonably approximate the characteristic parameters $r_m = 1.46$ mm and $f_m = 0.01$. Results at other times during the simulation are equally as good.

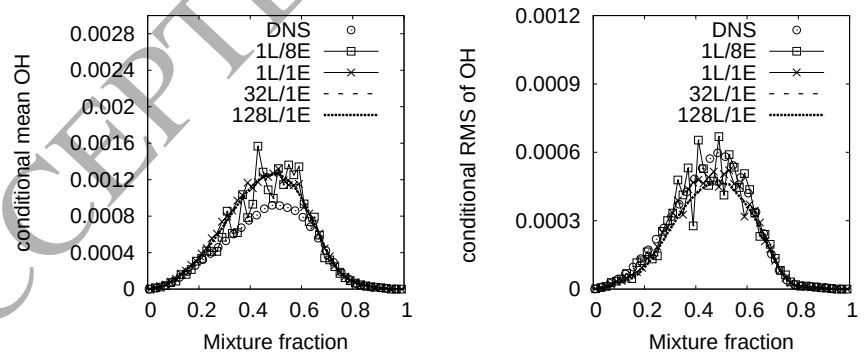

(a) (b)

Figure 8: Conditional (a) mean, and (b) RMS of OH mass fraction at $t/t_j = 20$.

Figure 8 presents the numerical convergence of the mean and RMS of hydroxyl mass fraction conditioned on the mixture fraction, Z. It is a fast radical species that forms in very thin layers near the stoichiometric mixture fraction and an ability to accurately capture it is the sign of a good model. In the figure the order of magnitude of the first and second conditional moments is quite insensitive to the particle number but the plots show a noticeable stochastic error for 1L/8E. Most importantly there is no bias error from using so few particles and, as expected, the stochastic error continuously decreased as more particles are employed and numerical convergence is obtained. The RMS is quite accurately predicted relative to the DNS data but the conditional mean is overpredicted and the reasons for this are not immediately obvious to us. The predictions of the major reactive scalars (not shown) exhibit a very similar numerical convergence behaviour and even better agreement with the DNS data. The present results are obtained with the new anisotropic time scale model given by Eq. (11) and this produces significantly better results for the reactive species than the original time scale model given by Eq. (10) which drastically underpredicts the conditional variances for all reactive scalars. The contrasting behaviour of the two different time scale models is analysed in [17].

4.3. Sandia Flame D: demonstration of numerical convergence in MMC-RANS

Numerical convergence is a conceptually much simpler prospect in dense MMC-RANS than it is in sparse MMC-LES. As reported in Sec. 4.2, the various Eulerian and Lagrangian filter scales in MMC-LES are model parameters and the model mixing time scale is directly linked to them. Great care is therefore required to ensure that the model parameters are held constant while numerical convergence is tested as $N_p \to \infty$. In MMC-RANS the Eulerian grid and Lagrangian particle loading are purely numerical parameters and the model mixing time scale is rightly independent of them. Since mixing in MMC-RANS is confined to the relatively large number of particles inside each grid cell (denoted N_{pc}), numerical convergence of the Lagrangian field is tested quite simply by increasing the number of particles while holding the RANS grid constant. Here

MMC-RANS is applied to Sandia flame D [34] which is a piloted methane/air flame exhibiting moderate levels of local extinction. In a previous MMC-RANS study [29] this flame, along with Sandia flames E and F which have higher levels of local extinction, was modelled with a focus on presenting the sensitivity of predictions to variations in the three primary model constants with $C_\phi = 2$, $b_o = \sqrt{1/2}$ and $r_t = 0.935$ being suggested as the most suitable values. It was also shown that flame F predictions did not vary substantially between a base case with $N_{\rm pc} = 70$, corresponding to $N_p = 268,800$ over the entire domain, and a refined case with twice that number. For completeness a systematic numerical convergence test should make one further increase by doubling the number of particles again. However, since flame F is close to blow-off the finite rate chemistry effects are strong and computations are expensive and that final level of convergence testing was not done. In the present work a systematic numerical convergence test is conducted for flame D which is considerably cheaper to model due to its composition being close to chemical equilibrium.

The experimental rig consists of a fuel jet surrounded by an annular pilot and a co-flow of air. The fuel is 25% methane and 75% air by volume whereas the pilot gases are combustion products. The jet and pilot diameters are $D = 7.2$ mm and $D_p = 18.2$ mm, respectively, and the jet velocity is 49.6 m/s corresponding to a jet Reynolds number of 22,400. The computational set-up uses an axisymmetric wedge mesh with an axial domain length of $50D$ and a radial length of $12.5D$. The mesh is nonuniform with 96 and 40 cells along axial and radial direction, respectively, with local refinement near the axis of symmetry and the fuel inlet. Testing has confirmed that predictions do not substantially change with further refinements of the grid [29]. A variable time step scheme based on a maximum Courant number of 0.8 is used in the present work and it has also been confirmed that results do not substantially change if lower values are used. As is standard, the $k-\varepsilon$ turbulence model constants are set to $C_{\epsilon 1} = 1.44$ and $C_{\epsilon 2} = 1.92$. Finite rate chemical kinetics are modelled using the DRM-19 mechanism [36].

Following the earlier flame F study, the base case computation in the present

work has $N_{\rm pc} = 70$ particles per cell and to systematically test the numerical convergence two levels of refinement are subsequently made with $N_{\rm pc} = 140$ and 280, corresponding to $N_p = 537,600$ and 1,075,200, respectively.

Figure 9 shows the radial profiles of the Favre mean and RMS of the mixture fraction, Z, at three different axial locations. There is negligible sensitivity of either the first or second moments towards $N_{\rm pc}$ at $x/D = 7.5$ and $x/D = 15$ while there is a very slight variation at $x/D = 30$. Additionally, the predictions are generally in good agreement with the experimental data at all locations. There is a small overprediction of the mean near the jet centreline at $x/D = 15$ and in the outer shear layer at $x/D = 30$ but as these minor differences with the data do not vary as the numerical solution converges they may be attributed to modelling issues.

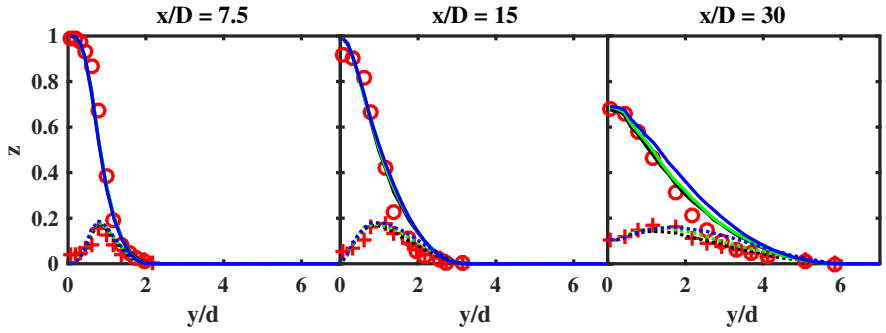

Figure 9: Sensitivity of radial profiles of mixture fraction mean and RMS to variation in the number of particles per cell at three different axial locations, $x/D = 7.5$ (left), $x/D = 15$ (centre) and $x/D = 30$ (right). Symbols: experiments; black line: $N_{pc} = 70$; green line: $N_{pc} = 140$; blue line: $N_{pc} = 280$. Circles and solid lines represent the mean whereas crosses and dotted lines represent the RMS.

In addition to the mixture fraction, Z, MMC-RANS also has a reference mixture fraction, f, which is modelled independently of Z, and thus the reactive species, according to Eq. (13). To ensure mixing is linear and independent with respect to all reactive species, the MMC mixing operation is local in f rather than Z. Although their mathematical independence means that f and

Z are stochastically different quantities, in order for f to be a useful localising quantity leading to accurate predictions of the reactive species there should be a strong correlation between the two. The correlation is controlled by the model constant r_t (a target value) and in a numerically converged solution the observed correlation should be independent of the number of particles. This is confirmed qualitatively by Fig. 10 which shows scatter plots of f versus Z and at each of the three axial locations the degree of correlation and the amount of dispersion around the conditional mean are not noticeably changed as $N_{\rm pc}$ is increased from 70 to 280. It may be noted that Z is strictly bounded between zero and one (as it should be) whereas f is unbounded on account of the random walk in its transport equation. For this reason f is only a reference variable rather than a true mixture fraction.

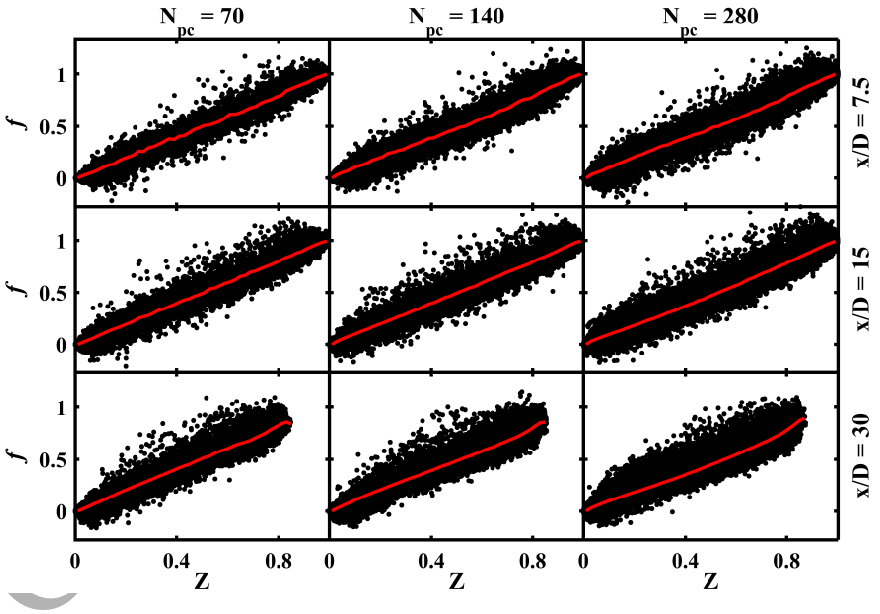

Figure 10: Scatter plots of f versus Z for different N_{pc} at $x/D = 7.5$ (top), $x/D = 15$ (centre) and $x/D = 30$ (bottom). 1^{st} column: $N_{\rm pc} = 70$; 2^{nd} column: $N_{\rm pc} = 140$; 3^{rd} column: $N_{\rm pc} = 280$; red line: conditional mean, $\langle f|Z\rangle$.

Conditional mean temperature profiles at the three axial locations are shown in Fig. 11. There is an exceptionally low sensitivity to the variation in $N_{\rm pc}$.

Furthermore, the predictions are in excellent agreement with the experimental data. The radial profiles of the (unconditional) Favre mean and RMS of temperature are presented in Fig. 12. Here there is a very slight variation in the results with increasing N_{pc} which, given the imperceptible sensitivity of the conditional mean in Fig. 11, may be associated with the also quite slight variations in the Z field with N_{pc} discussed above. There is good agreement with the experimental data at all axial and radial locations. Numerical convergence of the other reactive species (not shown for brevity) is similar to those presented here for temperature and overall the accuracy is good.

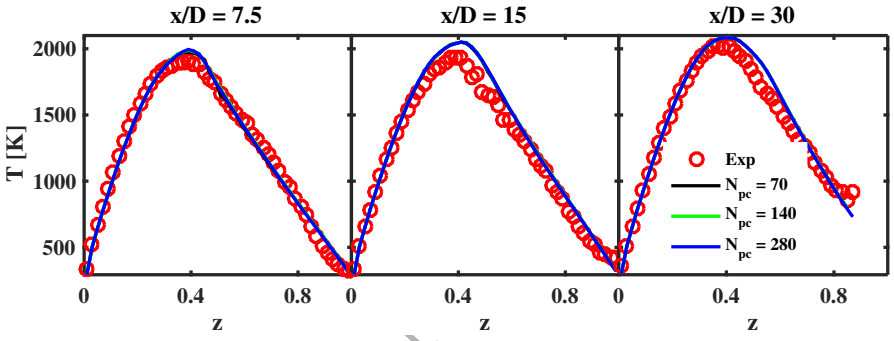

Figure 11: Sensitivity of conditional mean temperature to variation in the number of particles per cell at three different axial locations, $x/D = 7.5$ (left), $x/D = 15$ (centre) and $x/D = 30$ (right). Symbols: experiments; black line: $N_{\mathrm{pc}} = 70$; green line: $N_{\mathrm{pc}} = 140$; blue line: $N_{\mathrm{pc}} = 280$.

From the analysis above it is established that the leading order statistical moments of the conserved and reactive scalars are numerically converged for $N_{\mathrm{pc}} > 70$ and predictions are generally in good agreement with the experimental data.

4.4. Condensing dibutyl-phthalate jet flow: demonstration of numerical convergence and model sensitivity in the sectional form of MMC-LES

The previous three validation cases examined the numerical performance of MMC-LES and MMC-RANS for the turbulent transport of gaseous species only. This final validation case tests MMC-LES for the turbulent transport

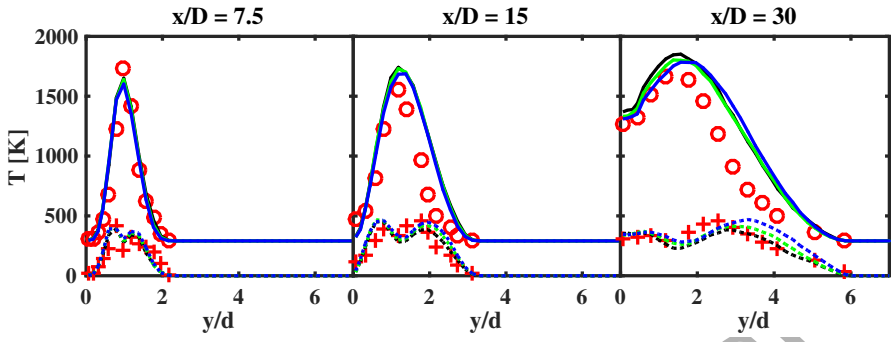

Figure 12: Sensitivity of radial profiles of temperature mean and RMS to variation in the number of particles per cell at three different axial locations, $x/D = 7.5$ (left), $x/D = 15$ (centre) and $x/D = 30$ (right) Symbols: experiments; black line: $N_{\mathrm{pc}} = 70$; green line: $N_{\mathrm{pc}} = 140$; blue line: $N_{\mathrm{pc}} = 280$. Circles and solid lines represent the mean whereas crosses and dotted lines represent the RMS.

of gaseous species and synthesised particulates which are modelled using the sectional method. The case was modelled previously in Neuber et al. [22]. In the present work two aspects of the computational approach are investigated; the numerical convergence of the particulate predictions with an increase in the number of sections, and the sensitivity of those predictions to variations in the characteristic mixing length scale, r_m. The first of these investigations was done in the earlier paper [22] and only the key details are repeated here. Testing the sensitivity to r_m is new and the results are reported in detail below. During that set of tests the primary model input parameter f_m is held constant and the variation in r_m effectively tests the sensitivity of the model to different levels of sparseness in the mixing model.

MMC-LES is applied to the experimental jet configuration reported by Lesniewski and Friedlander [35], where a hot nitrogen jet laden with gaseous dibutyl-phthalate (DBP) issues into a cold air stream. The turbulent mixing of the hot and cold streams leads to rapid cooling of the jet, inducing a super-saturated state and subsequent nucleation of particulates followed by surface growth. A variety of different jet conditions were investigated experimentally.

In the present simulations a reference case (*trial 824* in [37]) is used to perform the numerical convergence and sensitivity tests. It has a central jet of diameter $D = 2.35\,\mathrm{mm}$, bulk velocity $u_\mathrm{j} = 51.55\,\mathrm{m/s}$, temperature $T_\mathrm{j} = 413\,\mathrm{K}$ and DBP mole fraction of $x_{\mathrm{j,DBP}} = 3.6 \cdot 10^{-4}$. The corresponding jet Reynolds number is 4,700. The air coflow is at $T_\mathrm{c} = 299\,\mathrm{K}$ and has a velocity of $0.18\,\mathrm{m/s}$. Following the numerical trials, a subsequent very brief comparison is made to the experimental data for a range of cases with DBP loadings varying from $x_{\mathrm{jet,DBP}} = 2.5 \cdot 10^{-4}$ through to $5.1 \cdot 10^{-4}$ while all other parameters remain unchanged.

The simulation domain extends $70D$ axially and $31D$ in the radial direction. It has an LES mesh with 1.5 million cells and local refinement around the nozzle exit which has 39 cells across its diameter. Testing has confirmed that the predictions are quite insensitive towards further mesh refinement. The base configuration has $N_p = 480,000$ Pope particles corresponding to approximately 1 particle per 3 LES cells (1L/3E) and $r_m = 1.4$ mm. Although there are no chemical reactions in this case, nucleation and condensation are non-linearly dependent on the temperature which is determined by the turbulent mixing between the hot and cold streams. A reference variable is defined by a filtered mixture fraction whose value is one in the jet and zero in the coflow and we characterise the mixing distance in that reference mixture fraction space by $f_m = 0.03$ in all simulations. Homogeneous nucleation and particulate growth is modelled using the classical theory developed by Sutugin and Fuchs [38] and Girshick and Chiu [39] and the parameter settings reported in [22].

Convergence tests are conducted for variations in the number of sections in the particulate size distribution (PSD). The PSD is discretised into n_d sections and the nodal diameter of each section is d_p. In the first section $d_0 \approx 2.32\,\mathrm{nm}$ and subsequent sections have $d_k = c^k d_0$ where c is chosen to cover the entire size distribution up to a maximum of $d_\mathrm{max} \approx 10\,\mu\mathrm{m}$. Numerical convergence was tested by increasing n_d from 60 to 90 and then finally to 120 sections. Fig. 13 shows the predicted PSDs at an axial location of $z/D = 20$ above the nozzle. The sensitivity to n_d is generally small across the range and there is almost

no difference between the $n_d = 90$ and $n_d = 120$ cases. Since the real particulates have a continuum of possible diameters but the nodal sectional method confines those sizes to fixed nodal values, the method inherently introduces a discretisation error which leads to an artificial broadening of the PSD. That broadening can be quantified by the logarithm of the geometric standard deviation, $\ln \sigma$, which is expected to converge to the exact value as $n_d \to \infty$. For the results shown in Fig. 13, we have $\ln \sigma = 0.91$ for $n_d = 60$ and it converges to $\ln \sigma = 0.85$ for both $n_d = 90$ and 120. Analysis reported in [22] finds that the numerically induced component of $\ln \sigma$ in these last two cases is six times smaller than the physical broadening of the PSD induced by surface growth and this is rather small compared to uncertainties of DPB nucleation and growth kinetics. Given that they are 25% cheaper to compute and that the results appear to be numerically converged the next set of results all use $n_d = 90$.

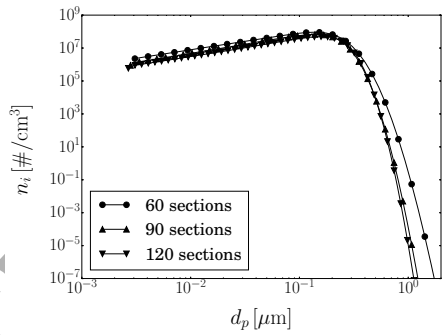

Figure 13: Sensitivity of particulate size distribution at $z/D = 20$ to variations in the number of sections. Figure adapted from [22] where these results were first reported.

The primary model input parameter is f_m and this controls the localness in reference mixture fraction space. r_m is a characteristic mixing length scale and generally model predictions are expected to be relatively insensitive to its exact value provided it remains in the inertial subrange of the turbulent spectrum [26, 17]. This expectation is tested here for predictions of particulate synthesis. Keeping $f_m = 0.03$ constant, r_m is reduced incrementally from its base case value of $r_m = 1.4$ mm down to $r_m = 0.7$ mm. This is achieved by increasing the

number of Pope particles by a factor of four from $N_p = 480,000$ to 1,920,000. This number is controlled in mmcFoam through the numerical parameter N_{pc} which is the number of particles in each cell of the `superMesh`. For the present configuration, $N_{\mathrm{pc}} = 25$ corresponds to $N_p = 480,000$ and $N_{\mathrm{pc}} = 100$ corresponds to $N_p = 1,920,000$. (Note that these are nominal values and stochastic variations occur during simulations.) Figs. 14(a) and 14(b) show the mean particulate number density (the first moment of the PSD) along the jet centreline and the PSD at $z/D = 20$, respectively. The sensitivity to N_{pc} and hence r_m is vanishingly small. The $N_{\mathrm{pc}} = 25$ case is of order four times cheaper to compute yet produces similar results to $N_{\mathrm{pc}} = 100$ (at least for these mean statistics).

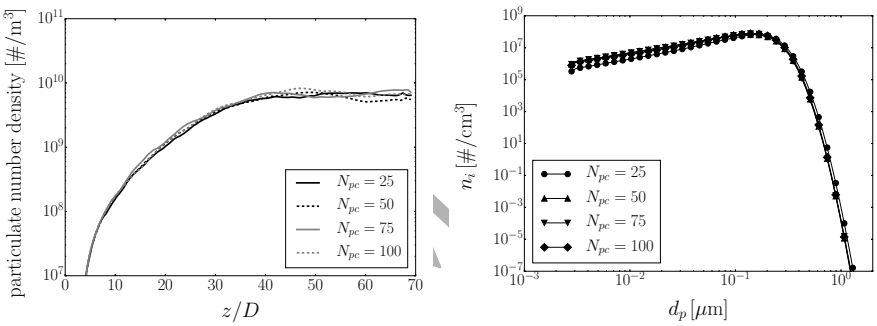

(a) (b)

Figure 14: (a) Sensitivity of axial mean particulate number density to variations in N_{pc} . (b) Sensitivity of particulate size distribution at $z/D = 20$ to variations in N_{pc}. Note that $N_{\mathrm{pc}} = 25$, 50, 75 and 100 correspond to $r_m = 1.4$ mm, 1.0 mm, 0.9 mm and 0.7 mm, respectively.

Finally, in Fig. 15 the MMC-LES model predictions of the mean number density of particulates as a function of DBP loading is compared to the experimental data at $z/D = 20$. The results are for $n_d = 90$ sections and $N_{\mathrm{pc}} = 50$ Pope particle per super cell. The simulations capture the measured trend correctly, but the slope is too steep and the dependence of the particulate number density on the DBP loading is overpredicted. This outcome is investigated thoroughly in Neuber et al. [22].

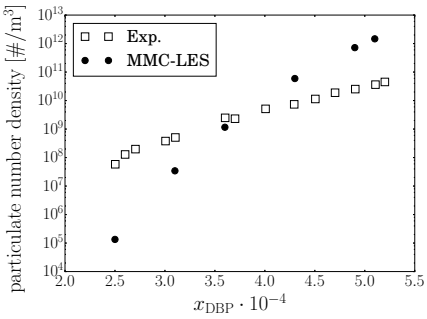

Figure 15: Mean particulate number density at $z/D = 20$ as function of the DBP mole fraction in the jet. Figure adapted from [22] where these results were first reported.

5. Conclusion

A stochastic version of the MMC model and its numerical implementation into a code known as mmcFoam have been described in detail. It incorporates a Monte Carlo method on an ensemble of Lagrangian (Pope) particles for simulating the turbulent reactive scalar fields that is coupled to a conventional Eulerian finite volume simulation of the LES or RANS continuity and Navier-Stokes equations.

The structure of mmcFoam is based on nested template class layers with each representing a particular physical aspect of turbulent combustion or aerosol particle synthesis. Those layers include `Advection`, `Thermo`, `Sectional`, `Mixing` and `Reacting`. Similar to the base OpenFOAM structure, `Submodels` are employed in mmcFoam to incorporate alternative physical models for each layer.

Four test cases with high quality experimental or DNS data were used here to validate the numerical implementation in mmcFoam. At the same time, mass consistency and numerical convergence are issues that affect all MMC-LES and MMC-RANS computational approaches, and the demonstrated success of the methods in achieving both consistency and convergence is not limited to this specific code. MMC-LES of the experimental Sydney piloted burner was per-

formed for both homogeneous and inhomogeneous inlet conditions to study mass consistency. The results demonstrated that the total mass and the distribution of that mass was consistent between the Eulerian and the Lagrangian schemes, confirming accurate numerical implementation of the density coupling method. It was found that both of the implemented density coupling submodels, known as `FlameletCurves` and `KernelEstimation`, generated consistent results while the improved numerical stability of the latter method was also explained. Numerical convergence as the number of Pope particles increased was explored for both MMC-LES and MMC-RANS. For MMC-LES this was studied against DNS data of a combusting syngas double shear layer configuration. In this case, the number of Pope particles was increased while the model parameters f_m and r_m were held constant. As a result, the mixing distances were independent of the number of particles while the sparse character of the mixing model was preserved. The results showed that the solution converged with a three order of magnitude increase in the number of Pope particles. This was followed by the simulation of Sandia flame D to confirm numerical convergence of the implemented MMC-RANS model. Simulations were performed for a base case and two refined cases, each having twice as many particles as the preceding one. Finally, a dibutyl-phthalate condensation case was considered to study the numerical performance of MMC-LES with both gaseous species and synthesised particulates which were modelled using the sectional method. In this case, the numerical convergence was tested for the variation of the number of sections in the particulate size distribution (PSD). The variation of characteristic mixing length scale, r_m, was also studied while the primary mixing input parameter, f_m, was held constant. The results confirmed that numerical convergence was achieved as the number of sections increased and that, as expected, the sensitivity of the model to r_m was small.

Acknowledgements

This work is funded by various Australian (ARC) and German (DFG) research council grants from 2013 - 2017, Universities Australia and Deutscher Akademischer Austausch Dienst under the Australia-Germany Joint Research Cooperation Scheme and the Colombian Administrative Department of Science, Technology and Innovation (COLCIENCIAS). We are grateful for figures on the syngas DNS shear layer provided by S. Vo. Computational resources were provided by the HPC services at Sydney (Artemis), Stuttgart (HLRS) and New South Wales.

References

References

[1] R. W. Bilger, S. Pope, K. Bray, J. Driscoll, Paradigms in turbulent combustion research, Proc. Combust. Inst. 30 (2005) 21–42.

[2] N. Peters, Laminar flamelet concepts in turbulent combustion, Symposium (International) on Combustion 21 (1) (1988) 1231–1250.

[3] S. B. Pope, PDF methods for turbulent reacting flows, Prog. Energy Combust. Sci. 11 (1985) 119–192.

[4] A. Klimenko, R. Bilger, Conditional moment closure for turbulent combustion, Prog. Energy Combust. Sci. 25 (6) (1999) 595–687.

[5] S. B. Pope, Lagrangian PDF methods for turbulent flows, Annu. Rev. Fluid Mech. 26 (1994) 23–63.

[6] A. Y. Klimenko, M. J. Cleary, Convergence to a model in sparse-Lagrangian FDF Simulations, Flow, Turbul. Combust. 85 (2010) 567–591.

[7] D. C. Haworth, Progress in probability density function methods for turbulent reacting flows, Prog. Energy Combust. Sci. 36 (2) (2010) 168–259.

[8] A. Y. Klimenko, S. B. Pope, The modeling of turbulent reactive flows based on multiple mapping conditioning, Phys. Fluids 15 (7) (2003) 1907–1925.

[9] S. Subramaniam, S. B. Pope, A mixing model for turbulent reactive flows based on Euclidean minimum spanning trees, Combust. Flame 115 (4) (1998) 487–514.

[10] A. Y. Klimenko, Matching conditional moments in PDF modelling of nonpremixed combustion, Combust. Flame 143 (4) (2005) 369–385.

[11] S. Pope, Mapping closures for turbulent mixing and reaction, Theoret. Comput. Fluid Dyn. 2 (1991) 255–270.

[12] A. Krisman, J. C. K. Tang, E. R. Hawkes, D. O. Lignell, J. H. Chen, A DNS evaluation of mixing models for transported PDF modelling of turbulent nonpremixed flames, Combust. Flame 161 (8) (2014) 2085–2106.

[13] C. Straub, S. De, A. Kronenburg, K. Vogiatzaki, The effect of time scale variation in multiple mapping conditioning mixing of PDF calculations for Sandia Flame series (D-F), Combust. Theor. Model. 20 (5).

[14] M. J. Cleary, A. Y. Klimenko, A generalised multiple mapping conditioning approach for turbulent combustion, Flow Turbul. Combust. 82 (4) (2009) 477–491.

[15] F. Gao, E. E. O'Brien, A large-eddy simulation scheme for turbulent reacting flows, Phys. Fluids A 5 (1993) 1282.

[16] M. J. Cleary, A. Y. Klimenko, J. Janicka, M. Pfitzner, A sparse-Lagrangian multiple mapping conditioning model for turbulent diffusion flames, Proc. Comb. Inst. 32 (1) (2009) 1499–1507.

[17] S. Vo, O. T. Stein, A. Kronenburg, M. J. Cleary, Assessment of mixing time scales for a sparse particle method, Combust. Flame 179 (2017) 280–299.

[18] H. Weller, G. Tabor, H. Jasak, C. Fureby, A tensorial approach to computational continuum mechanics using object-oriented techniques, Comput. Phys. 12 (1998) 620–631.

[19] B. Sundaram, A. Klimenko, M. Cleary, Y. Ge, A direct approach to generalised Multiple Mapping Conditioning for selected turbulent diffusion flame cases, Combust. Theor. Model. 20 (2016) 735–764.

[20] S. Galindo, F. Salehi, M. J. Cleary, A. R. Masri, MMC-LES simulations of turbulent piloted flames with varying levels of inlet inhomogeneity, Proc. Combust. Inst. 36 (2017) 1759–1766.

[21] F. Salehi, M. J. Cleary, A. R. Masri, Y. Ge, A. Y. Klimenko, Sparse-Lagrangian MMC simulations of an n-dodecane jet at engine-relevant conditions, Proc. Comb. Inst. 36 (2017) 3577–3585.

[22] G. Neuber, A. Kronenburg, O. T. Stein, M. J. Cleary, MMC-LES modelling of droplet nucleation and growth in turbulent jets, Chem. Eng. Sci. 167 (2017) 204–218.

[23] A. Varna, M. J. Cleary, E. R. Hawkes, A multiple mapping conditioning mixing model with a mixture-fraction like reference variable. Part 1: Model derivation and ideal flow test cases, Combust. Flame 181 (2017) 342–353.

[24] S. Vo, A. Kronenburg, O. T. Stein, M. J. Cleary, Multiple mapping conditioning for silica nanoparticle nucleation in turbulent flows, Proc. Combust. Inst. 36 (2017) 1089–1097.

[25] OpenFOAM, www.openfoam.org, 2017.

[26] M. J. Cleary, A. Y. Klimenko, A detailed quantitative analysis of sparse-Lagrangian filtered density function simulations in constant and variable density reacting jet flows, Phys. Fluids 23 (11) (2011) 115102.

[27] J. H. Friedman, J. L. Bentley, R. A. Finkel, An algorithm for finding best matches in logarithmic expected time, ACM Transactions on Mathematical Software (TOMS) 3 (3) (1977) 209–226.

[28] Y. Ge, M. J. Cleary, A. Y. Klimenko, A comparative study of Sandia flame series (D-F) using sparse-Lagrangian MMC modelling, Proc. Comb. Inst. 34 (1) (2013) 1325–1332.

[29] A. Varna, M. J. Cleary, E. R. Hawkes, A multiple mapping conditioning mixing model with a mixture-fraction like reference variable. Part 2: RANS implementation and validation against a turbulent jet flame, Combust. Flame 181 (2017) 354–364.

[30] M. Muradoglu, S. B. Pope, D. A. Caughey, The hybrid method for the PDF equations of turbulent reactive flows: consistency conditions and correction algorithms, J. Comput. Phys. 172 (2) (2001) 841–878.

[31] J. J. Monaghan, Smoothed particle hydrodynamics, Rep. Prog. Phys. 68 (8) (2005) 1703.

[32] S. B. Pope, A model for turbulent mixing based on shadow-position conditioning, Phys. Fluids 25 (11) (2013) 110803.

[33] S. Meares, A. R. Masri, A modified piloted burner for stabilizing turbulent flames of inhomogeneous mixtures, Combust. Flame 161 (2) (2014) 484–495.

[34] R. Barlow, J. Frank, Effects of turbulence on species mass fractions in methane/air jet flames, Symposium (International) on Combustion 27 (1) (1998) 1087–1095.

[35] T. Lesniewski, S. Friedlander, Particle nucleation and growth in a free turbulent jet, Proc. Royal. Soc. A. 454 (1998) 2477–2504.

[36] A. Kazakov, M. Frenklach, Avaiable at:http://www.me.berkeley.edu/drm/.

[37] T. Lesniewski, Particle nucleation and growth in turbulent jets, Ph.D. thesis, University of California, Los Angeles (1997).

[38] A. Sutugin, N. Fuchs, Formation of condensation aerosols at high vapor saturation, J. Colloid Interf. Sci 27 (1968) 216 228.

[39] S. Girshick, C. Chiu, Kinetic nucleation theory: a new expression for the rate of homogeneous nucleation from an ideal supersaturated vapor, L. Chem. Phys. 93 (1990) 1273 – 1277.

[40] P. E. Kloeden, E. Platen, Numerical Solution of Stochastic Differential Equations, Applications of Mathematics, Stochastic Modelling and Applied Probability, Vol. 23, Springer, New York, 1995.

[41] R. L. Curl, Dispersed phase mixing: I. Theory and effects in simple reactors, AIChE Journal 9 (2) (1963) 175–181.

[42] M. Sirignano, J. Kent, A. D'Anna, Modeling formation and oxidation of soot in nonpremixed flames, Energy Fuel 27 (2013) 2303 – 2315.

Appendix A. Relevant details of the mmcFoam template class layers

The heirarchical structure of mmcFoam with its nested template layers is described in Section 3. This appendix contains specific details of each layer, including information about submodel physics, numerical schemes, boundary conditions, meshing and Pope particle number control.

Appendix A.1. `Advection` template class layer

This layer handles advective movement of `PopeParticles`, their initialisation and boundary conditions, and their spatial resolution.

Advective transport occurs in a Lagrangian sense by integration of Eq. (1) using a temporally first-order Euler-Maruyama scheme [40]. The filtered velocity and density and the effective diffusivity are estimated at the particle locations by tri-linear interpolation from the three-dimensional finite volume fields. `PopeParticles` enter and leave the computational domain at boundary `patches`. Inflows are controlled by the `InflowBoundary` submodel. Presently the `FreeStream` option is implemented whereby `PopeParticles` enter the domain after being accumulated on the boundary with a mass flow that is equivalent to the inflow mass flux on the LES or RANS finite volume `mesh`.

At solid walls PopeParticles are rebounded with a consistent wall-normal displacement.

In addition to the standard finite volume mesh for solving the LES/RANS equations, a superMesh is defined to control the particle resolution. This is shown schematically in Fig A.16 where the LES/RANS mesh is represented by thin lines and the superMesh by thick lines. In the figure, which depicts a sparse simulation, the superMesh is the coarser of the two meshes and there are fewer PopeParticles (represented by points) than mesh cells. In dense simulations the two meshes can be the same. The number of PopeParticles is controlled on the superMesh within a specified range. It is emphasised that Eulerian flow properties are registered to the mesh and the superMesh is only employed for particle number control. At initialisation PopeParticles are randomly distributed and their mass is stochastically equivalent to that of the Eulerian field. Since it is a mass density function method, as the simulation proceeds the PopeParticles will tend to redistribute according the density and this may not coincide with the required resolution. A number control algorithm is employed whereby PopeParticles are cloned or killed if the number falls below or above the lower and upper limits, respectively. Cloning is achieved by halving the mass of an existing particle and then replicating it. Killing is achieved by doubling the mass of an existing particle and then deleting it from memory with a 50% probability. To alleviate situations where particle mass disparity becomes unbalanced the cloning is weighted towards heavier particles while killing is weighted towards lighter particles.

Appendix A.2. Thermo template class layer

The Thermo layer encapsulates the composition properties of the PopeParticles, thus all variables related to the thermochemical state are template class members, including species mass fractions, standardised enthalpy, pressure, temperature and the sensible enthalpy. It is noted that the last three scalars are not transported quantities and while they are members of this layer they are not part of the TPDFData class.

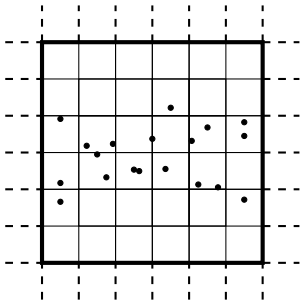

Figure A.16: Cloud In Super Cell for sparse Lagrangian simulations

The modelling of the composition, radiation and density coupling are controlled by `Submodels` in the `Thermo` layer. Presently the composition modelling is derived from OpenFOAM's `SinglePhaseMixture` submodel and the radiation is modelled according to the optically thin assumption. As discussed in detail in Section 2.4 two density coupling methods are available in the code; namely the `FlameletCurves` submodel and the `KernelEstimation` submodel.

Appendix A.3. `Sectional` template class layer

This layer handles the methods specific to the turbulent transport of the number density of synthesised particulates, $\boldsymbol{N}$. The particle size distribution (PSD) is divided into sections that represent discrete nodal values of the diameter. For the particulate quantities the source term, W_α, in Eq. (2) describes the changes to the PSD due to interactions with the gas phase and these are implemented conventiently through the `Submodels`. Presently a model called `HomogeneousNucleationGrowth` treats nucleation and growth according to the classical theory developed by Sutugin and Fuchs [38] and Girshick and Chiu [39] and recently tested in Neuber et al. [22]. As the particulate species nucleate and grow their calculated diameter at any instant will not, in general, naturally coincide with the preset nodal values of the particulate sections. The increment in the number density for each section, dN_α, is therefore distributed between adjacent nodes with a weighting that ensures that mass is conserved although

consequently some artificial broadening of the size distribution is introduced.

Appendix A.4. `Mixing` template class layer

Mixing is the only multipoint operation performed on the `PopeParticles` resulting in an exchange of scalar information between them. Both dense and sparse mixing schemes have been implemented via the `Submodels` for this class. The `MMCCurl` submodel is applicable to both dense and sparse schemes while the `Curl` submodel, which follows the standard Curl's mixing model [41], is applicable only to dense simulations.

Appendix A.5. `Reacting` template class layer

The `Reacting` template class deals with the variation in composition due to homogeneous gas-phase reactions. Presently two finite rate kinetics and one fast chemistry `Submodels` are available. In the former grouping there is `finiteRateParticleReaction` which integrates the composition of the `PopeParticles` using the various stiff ODE solvers that are available in OpenFOAM's `chemistrySolver` class. Additionally there is `sootParticleReaction` which incorporates both gaseous and sooting species according the multisectional method described by Sirignano et al. [42]. In the latter group a Burke-Schumann flamesheet fast chemistry model that is described in [26] implemented in the `flameSheetParticleReaction` method.